Original Article

Characterizing PANoptosis gene signature in prognosis and chemosensitivity of colorectal cancer

Tingyu Zhao[1#], Xiao Zhang[1#], Xiao Liu[2], Xingyu Jiang[1], Silu Chen[2], Huiqin Li[2], Hongsheng Ji[2], Sumeng Wang[1], Qi Liang[1], Siqi Ni[1], Mulong Du[2], Lingxiang Liu[1]

[1]Department of Oncology, The First Affiliated Hospital of Nanjing Medical University, Nanjing, China; [2]Department of Environmental Genomics, Jiangsu Key Laboratory of Cancer Biomarkers, Prevention and Treatment, Collaborative Innovation Center for Cancer Personalized Medicine, School of Public Health, Nanjing Medical University, Nanjing, China

Contributions: (I) Conception and design: L Liu, T Zhao, X Zhang; (II) Administrative support: L Liu; (III) Provision of study materials or patients: M Du, S Chen, H Li, H Ji; (IV) Collection and assembly of data: X Liu, S Wang, Q Liang, S Ni; (V) Data analysis and interpretation: T Zhao, X Zhang; (VI) Manuscript writing: All authors; (VII) Final approval of manuscript: All authors.

[#]These authors contributed equally to this work.

Correspondence to: Mulong Du, MD. Department of Environmental Genomics, Jiangsu Key Laboratory of Cancer Biomarkers, Prevention and Treatment, Collaborative Innovation Center for Cancer Personalized Medicine, School of Public Health, Nanjing Medical University, 101 Longmian Avenue, Jiangning District, Nanjing 211166, China. Email: drdumulong@njmu.edu.cn; Lingxiang Liu, MD. Department of Oncology, The First Affiliated Hospital of Nanjing Medical University, 300 Guangzhou Road, Nanjing 210029, China. Email: llxlau@163.com.

Background: PANoptosis is a cell death pathway involved in pyroptosis, apoptosis and necrosis, and plays a key role in the development of malignant tumors. However, the molecular signature of PANoptosis in colorectal cancer (CRC) prognosis has not been thoroughly explored. The present study aimed to develop a novel prognostic model based on PANoptosis-related genes in CRC.

Methods: We initially included transcriptome data of 404 CRC samples from The Cancer Genome Atlas (TCGA) cohort and identified differentially expressed genes related to PANoptosis. We then employed Cox, least absolute shrinkage and selection operator (LASSO) regression, and Random Forest methods to determine the prognostic value and constructed a PANoptosis prognostic model, followed by the validation on both internal (TCGA) and external datasets [Nanjing Colorectal Cancer (NJCRC) and Gene Expression Omnibus (GEO), n=635]. We performed immune infiltration analysis and gene set enrichment analysis to reveal biological processes and pathways against differential risk score. Ultimately, we carried out drug sensitivity analysis to predict the response of CRC patients to diverse treatment strategies.

Results: We constructed a predictive model based on four PANoptosis-related genes (*TIMP1*, *CDKN2A*, *CAMK2B*, and *TLR3*), with a high performance [area under the curve (AUC)$_{1\text{-year}}$ =0.702, AUC$_{3\text{-year}}$ =0.725, AUC$_{5\text{-year}}$ =0.668] and being an independent prognostic factor in predicting the prognosis of CRC patients. Notably, colorectal tumor with high PANoptosis risk score performed higher levels of macrophage infiltration and immune scores, but a greater reduction of Tumor Microenvironment Score (TMEscore) and DNA replication. Particularly, patients in high-risk group exhibited higher sensitivity to fluorouracil, oxaliplatin and lapatinib compared to the low-risk group.

Conclusions: This study highlights the prognostic potential of PANoptosis-related features in CRC, demonstrating their role as key biomarkers significantly associated with patient survival and aiding in the identification of high-risk patients, thereby advancing immunotherapy approaches.

Keywords: Colorectal cancer (CRC); PANoptosis; prognosis

Submitted Apr 05, 2024. Accepted for publication Sep 09, 2024. Published online Oct 29, 2024.
doi: 10.21037/jgo-24-245
View this article at: https://dx.doi.org/10.21037/jgo-24-245

Introduction

Colorectal cancer (CRC) ranks as the second most frequently diagnosed cancer (1). Cornerstone treatments for CRC are often accompanied by a spectrum of side effects, including physical discomfort, drug resistance, recurrence, metastasis, and treatment intolerance. These challenges underscore the urgent need for treatments that are not only minimally invasive but also precise and efficient. The 2021 National Comprehensive Cancer Network guidelines emphasize the significance of assessing seven key biomarkers [*KRAS*, *NRAS*, *BRAF*, microsatellite instability (*MSI*), mismatch repair (*MMR*), *ERBB2* amplification, and *NTRK* fusion] to guide optimal clinical decisions (2). Comprehensive genomic studies across large cohorts have shed light on the molecular landscape of both early-stage and metastatic CRC, facilitating the development of patient-specific treatments anchored in their unique molecular profiles (3,4). Notably, mutations in KRAS and BRAF have been identified as indicators of poor response to epidermal growth factor receptor inhibitors, which correlate with reduced overall and progression-free survival rates. Alarmingly, despite advancements in chemotherapy, targeted treatments, and immunotherapy, recurrence or metastasis remains a significant concern, affecting up to one-third of patients with stage I–III CRC and a staggering 65% of those diagnosed with stage IV CRC (5). Hence, a more profound investigation in this domain is paramount to establish a sound foundation for its clinical diagnosis and treatment strategies.

PANoptosis, a comprehensive inflammatory cell death mechanism, integrates three distinct programmed cell death (PCD) pathways. This concept was first introduced by Malireddi *et al.* in 2019 (6). Being a fusion of Pyroptosis (P), Apoptosis (A), and Necroptosis (N), the nomenclature accentuates its complex nature, and offers a panoramic perspective on cell death by highlighting the synergy among these processes (7,8). Aberrant regulation of PANoptosis has been implicated in a myriad of human diseases, spanning from autoimmune inflammatory disorders to infectious diseases, metabolic conditions, and even cancers (9). Caspase-6, a central biomarker closely intertwined with PANoptosis, is pivotal in amplifying ZBP1-mediated inflammasome activation, cellular apoptosis, and host defense mechanisms during influenza A virus (IAV) infection. Intriguingly, in a mouse model subjected to IAV infection, caspase-6 deficiency hinders PANoptosis activation, resulting in diminished viral elimination (10). In the context of adrenocortical carcinoma (ACC), CDK1 modulates the PANoptosis through a ZBP1-dependent mechanism, subsequently influencing the proliferation of ACC cells (11).

In oncology research, the roles of pyroptosis, apoptosis, and necroptosis remain subjects of intense debate. Depending on the context, these processes can either inhibit tumor progression or promote tumorigenesis. For instance, a decrease in key molecules of necroptosis such as MLKL, is correlated with unfavorable outcomes in multiple malignancies, including CRC, acute myeloid leukemia, and breast cancer. Conversely, increased expression of RIPK3 or RIPK1 is also associated with a positive outcome in both lung and pancreatic malignancies (12). Previous studies have revealed that inhibiting necroptosis can not only enhance cancer cell proliferation but also lead to aggressive malignancies (12). The absence of RIPK3 or the inhibition of RIPK1 in pancreatic cancer models demonstrated a suppressive effect on tumor formation, further suggesting that necroptosis might promote tumorigenesis in certain contexts (13). In summary, albeit necroptosis can initiate cancer cell mortality, it can also trigger inflammation response, and promote cancer development. Impaired cellular apoptosis can prolong tumor cell survival, leading to the accumulation of mutations that drive tumor progression, including proliferation and metastasis. Numerous

Highlight box

Key findings

- *TIMP1*, *CDKN2A*, *CAMK2B*, and *TLR3* are identified as critical PANoptosis-related genes in colorectal cancer (CRC), significantly influencing patient prognosis and chemotherapeutic sensitivity.

What is known and what is new?

- PANoptosis is a cell death pathway integrating pyroptosis, apoptosis, and necroptosis, playing a role in cancer progression.
- This study is the first to establish a prognostic model based on PANoptosis-related genes in CRC, offering a new method for predicting patient outcomes and treatment responses.

What is the implication, and what should change now?

- PANoptosis-related gene signatures, particularly *TIMP1*, *CDKN2A*, *CAMK2B*, and *TLR3*, should be considered in developing personalized treatment strategies for CRC.
- These findings support the need for incorporating PANoptosis-related gene profiling into CRC clinical management to improve prognosis prediction and optimize therapeutic approaches.

anticancer agents that can induce cellular apoptosis, like interferons (IFNs) with nuclear export inhibitors or tumor necrosis factor (TNF) with IFN-γ, have demonstrated their potential in combating cancer (14,15). The combination of IFN and KPT can evoke ZBP1-dependent PANoptosis, thereby inhibiting the growth of melanoma in mice. The PANoptosis triggered by IFN and KPT correlates with the unique human protein ADAR1 that has a Zα domain. The interaction of ZBP1 with ADAR1 sustains cell survival, but its binding with RIPK3 also leads to cell demise (15). Moreover, in melanoma mouse experimental models, cell apoptosis caused by ZBP1 can elevate the responsiveness to immune checkpoint inhibitor therapies (16). Genes related to PANoptosis, such as *ZBP1*, are associated with a favorable prognosis in patients with melanoma. The PANoptosis induced by the combination of TNF and IFN-γ has shown preclinical promise in reducing tumor size in mouse xenograft models (17). In conclusion, while the effect of pyroptosis and necroptosis in tumor progression remain inconsistent, drugs inducing PANoptosis exhibit significant potential in cancer treatment (18). As a CDK1 inhibitor, cucurbitacin E (CurE), can suppress ACC cell proliferation by eliciting PANoptosis in those cells both *in vitro* and *in vivo* (11). Sulconazole leads to PANoptosis by initiating oxidative stress and halting glycolysis, subsequently increasing the sensitivity of esophageal cancer to radiation therapy (19). Namely, a thorough exploration of the mechanisms of PANoptosis presents new possibilities for formulating more effective treatment plans for CRC patients (8). Therefore, a comprehensive study of the role of PANoptosis in the progression of CRC is warranted.

In this study, we analyzed the mRNA expression dataset from The Cancer Genome Atlas (TCGA) database, profiling hallmark gene sets in 404 cases of CRC. We identified PANoptosis-related key genes and constructed a prognostic model based on these genes. The model demonstrated high predictive accuracy for CRC prognosis, with significant associations found between high PANoptosis risk scores and poorer survival outcomes. Additionally, our study highlighted the potential of these genes as biomarkers for CRC diagnosis and prognosis, offering insights into the molecular mechanisms underlying CRC progression and aiding in the advancement of personalized treatment strategies. We present this article in accordance with the TRIPOD reporting checklist (available at https://jgo.amegroups.com/article/view/10.21037/jgo-24-245/rc).

Methods

Data acquisition

We obtained gene expression and medical information of CRC patients from TCGA database (https://cancergenome.nih.gov/). Initially, 434 patients were selected for analysis. Patients with incomplete clinical and follow-up information or duplicates were excluded. Consequently, 404 samples were included for subsequent studies. Nanjing Colorectal Cancer (NJCRC) cohort and GSE39582 (https://www.genome.gov/) supported available data of CRC for validation as appropriate (20). We combined NJCRC and GSE39582 to create an external validation set of 635 samples. Batch effects are removed prior to analysis. Clinical characteristics were detailed in Table S1. The study was conducted in accordance with the Declaration of Helsinki (as revised in 2013).

Screening of differentially expressed genes (DEGs) related to CRC and PANoptosis

To obtain a comprehensive PANoptosis gene list, we searched multiple databases for genes related to pyroptosis, apoptosis, and necroptosis and retain nonduplicate ones. Specifically, the list of pyroptosis genes was sourced from the Reactome pathway database, the set of necroptosis genes originated from the Kyoto Encyclopedia of Genes and Genomes (KEGG) database, and the list of apoptosis genes was a combination of data from the HALLMARK, REACTOME, and KEGG pathway databases. In total, 485 non-redundant genes were identified and included for further analysis (Table S2).

DEGs between the normal and cancer groups was detected using the 'limma' package (version 3.40.6). A linear model to the expression data was fitted using the lmFit function in conjunction with a design matrix. Subsequently, an empirical Bayes method was employed to adjust the standard errors of these fits. The criteria for identifying DEGs were set at $P<0.05$ and $|\log2 \text{ fold change (FC)}| >1$. Following the filtering process, 88 PANoptosis-related DEGs were pinpointed for further validation (Table S3).

Construction of a prognostic model by PANoptosis-related DEGs

We initially explored the association of individual genes with

patient survival duration using a univariate Cox regression model, identifying a set of genes significantly associated with survival outcomes. Afterwards, the least absolute shrinkage and selection operator (LASSO) regression technique was employed with the aim of isolating the most prognostically impactful gene features. Through meticulous cross-validation and Bootstrap resampling procedures, the optimal regularization parameter λ was accurately determined. Based on this parameter, a set of gene features correlated to survival time was identified. In the subsequent phase of the analysis, we implemented random forest algorithm for feature selection. After repeated Bootstrap resampling and cross-validation procedures, we derived the average significance of each trait to determine the most important genetic signature Finally, a intersection of gene features identified by the aforementioned three methods was determined as hub genes, which would be involved in the prognostic model for CRC.

Ultimately, the LASSO regularization was combined with multivariate Cox regression to construct a prognostic model, further verifying the correlation of these feature genes with the prognosis of CRC patients. The computational formula that weight the expression values of hub genes with the regression coefficients was as follows:

The risk score = $\sum$(−0.2590) × (TLR3 expression) + (0.0638) × (CDKN2A expression) + (0.1319) × (CAMK2B expression) + (0.4802) × (TIMP1 expression).

Based on the risk score, we categorized clinical samples into high-risk and low-risk groups to thoroughly assess the predictive efficacy of the model.

Validation of prognostic model

Survival curves were plotted utilizing Kaplan-Meier method. Three variables were selected for analysis: risk score, pathological staging, and age, which exhibited significant association with patient survival in univariate Cox regression analysis. Following the foundation of the univariate analysis, a multivariate Cox regression model was executed to investigate the joint effects of the mentioned variables on the survival duration of patients. To delve deeper into the predictive performance of the risk score, we utilized the 'survivalroc' function to draw receiver operating characteristic (ROC) curves at the 1-, 3-, and 5-year marks, using the area under the curve (AUC) value as the measure of prediction precision. To verify the robustness and generalizability of our risk model, the aforementioned procedures were reiterated using an independent test set. We then combined t-tests, box plots, and Kaplan-Meier survival curves to comprehensively assess the clinical relevance of the risk scores across different patient subgroups.

Exploration of immune cell infiltration and the tumor immune microenvironment

To explore and contrast the infiltration rates of 22 immune cell types in high-risk versus low-risk groups, we utilized three computational techniques: CIBERSORTx, ImmuneCellAI, and single-sample gene set enrichment analysis (ssGSEA). To further understand the connection between the tumor microenvironment (TME) and the risk score, we undertook correlation studies using methods like TMEscore, Estimate, and ssGSEA.

Functional enrichment analysis

We employed functional enrichment analysis and GSEA to characterize the molecular and biological functions of the risk model. GSEA (version 4.1.0) (https://www.broadinstitute.org/gsea/index.jsp) was utilized to evaluate the differential gene expression between high-risk and low-risk groups, identifying associated biological pathways and functions.

Drug sensitivity analysis

In search of therapeutic drugs effective for patients, we carried out a drug reactivity analysis using the 'oncoPredict' software package. We investigated the association between drug reactivity and parameters like risk scores, TIMP1, CDKN2A, CAMK2B, and TLR3.

Statistical analysis

All statistical analyses were performed using R (version 4.0.5) software (https://www.r-project.org/). P values <0.05 were considered significant.

Results

Identification and functional analysis of PANoptosis-related DEGs for CRC

The workflow adopted for the analysis of PANoptosis-related gene markers is delineated in *Figure 1*. Differential

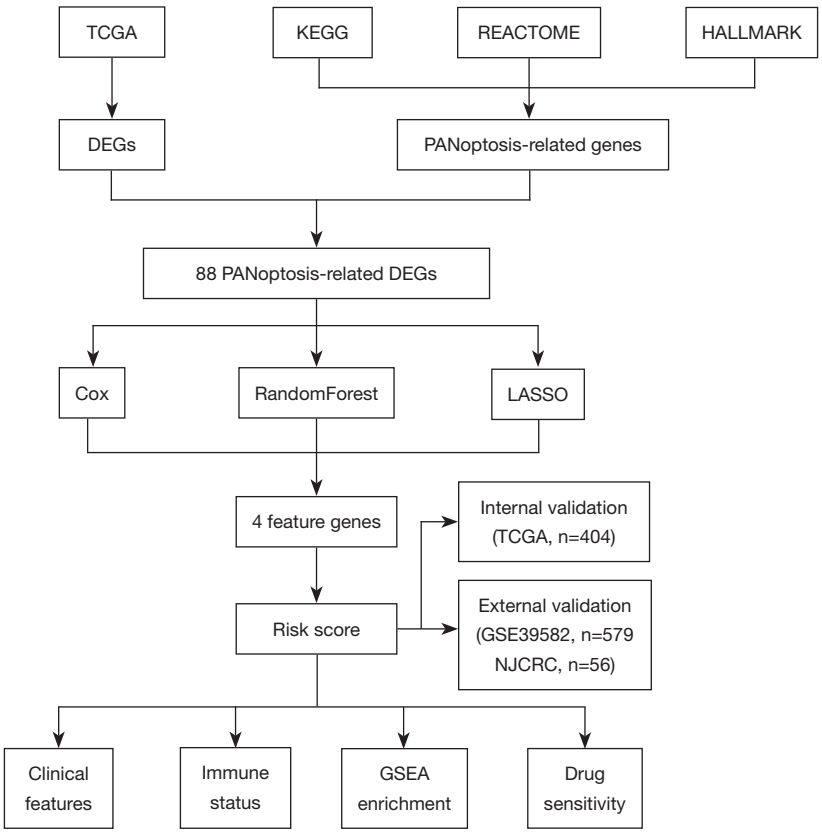

Figure 1 Flow diagram of the study. TCGA, The Cancer Genome Atlas; KEGG, Kyoto Encyclopedia of Genes and Genomes; DEGs, differentially expressed genes; LASSO, least absolute shrinkage and selection operator; NJCRC, Nanjing Colorectal Cancer; GSEA, gene set enrichment analysis.

gene expression analysis between normal and tumor samples derived from TCGA cohort revealed a total of 444 DEGs ($P<0.05$, logFC>1). From databases including KEGG, REACTOME, and HALLMARK, we retrieved 485 genes associated with PANoptosis. By intersecting the DEGs with the PANoptosis-associated genes, we discerned 88 PANoptosis-related DEGs.

Screening of PANoptosis-related and prognostic genes

Firstly, we assessed the association of each gene with survival duration, using univariate Cox regression analysis and identified 11 significant results (*Figure 2A*). Then, we employed LASSO regression. As for cross-validation, the optimal regularization parameter λ was determined to be 0.038, and the final LASSO model was established based on this parameter (*Figure 2B*,*2C*). This model yielded a set of genes with non-zero coefficients, with these 11 genes deemed to be most associated with survival duration (*Figure 2D*). Simultaneously, we performed feature selection using random forests, a tree-based method, to get an importance score for each feature. We subjected these scores to multiple Bootstrap iterations and cross-validations to derive the average importance score for each feature. In accordance with these scores, the top 10 most important features were identified (*Figure 2E*). Ultimately, the intersection of the three methods yielded four selected genes for subsequent analyses (*Figure 2F*). Three genes (*TIMP1*, *CDKN2A*, and *CAMK2B*) were defined as adverse prognostic factors (*Figure 2G-2I*), while TLR3 was favorable for prognosis (*Figure 2J*).

Establishment and validation of a PANoptosis-related prognostic model

We utilized samples from the TCGA database as our train set and constructed a prognostic model by integrating LASSO regularization with multivariate Cox regression.

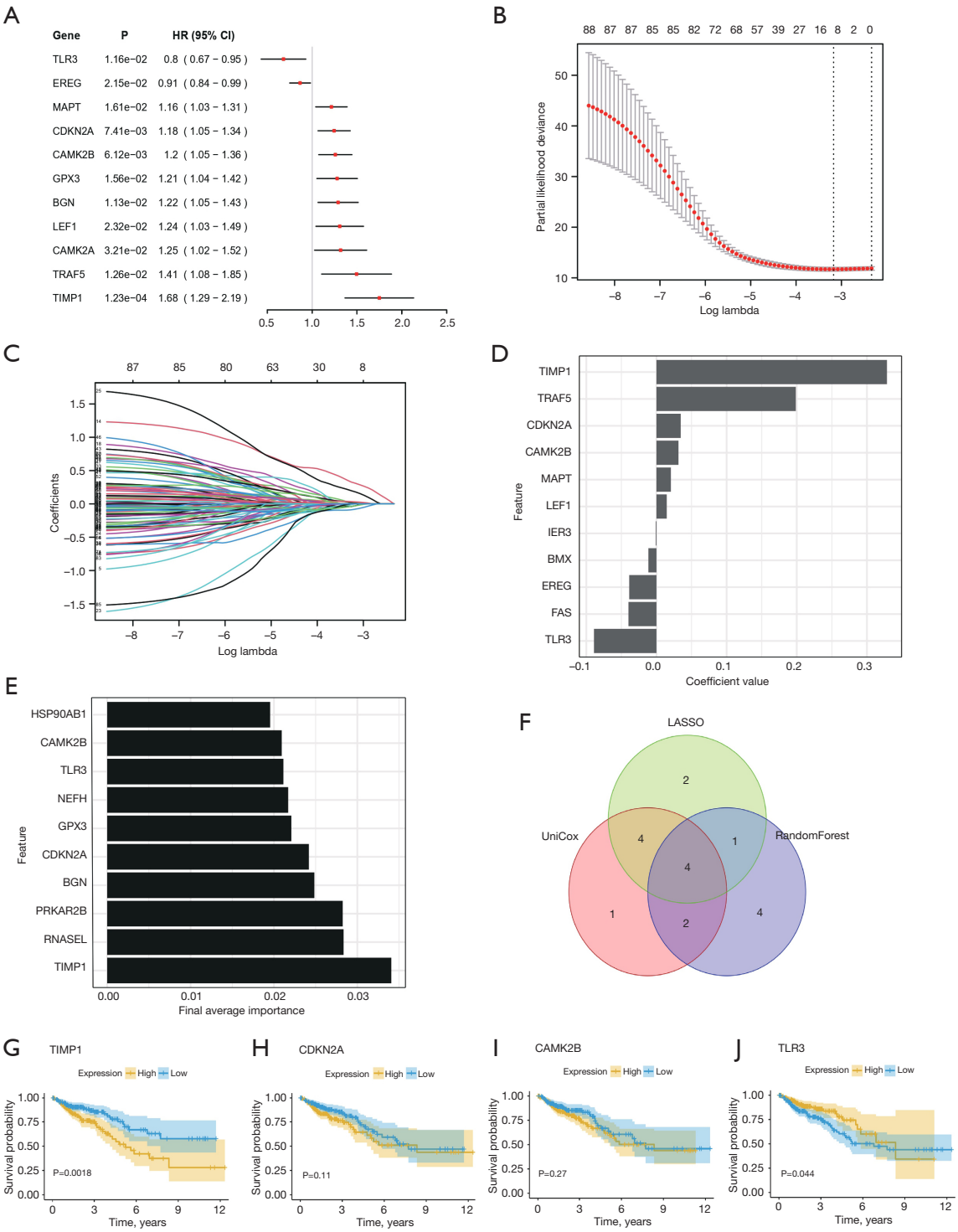

Figure 2 Identification of prognostic-related genes in patients with CRC. (A) Univariable cox regression analysis of 11 prognostic genes. (B) Cross-validation curve for LASSO regression. (C) The LASSO coefficient path of 88 genes. (D) Non-zero coefficients from LASSO model. (E) Top ten features based on final average importance from random forest algorithm. (F) Venn diagram presenting the feature genes selected by three methods. (G-J) Survival curve of patients with CRC in different groups. LASSO, single-sample gene set enrichment analysis; HR, hazard ratio; UniCox, universal Cox proportional hazards model; CRC, colorectal cancer.

The risk score was calculated using the formula: ∑(–0.2590) × (TLR3 expression) + (0.0638) × (CDKN2A expression) + (0.1319) × (CAMK2B expression) + (0.4802) × (TIMP1 expression). Based on the risk score, samples were further stratified into high-risk and low-risk groups. Compared to the low-risk group, patients in the high-risk group exhibited significantly poorer survival outcomes (P<0.001) (*Figure 3A*). In the univariate and multivariate Cox regression studies of the training set, we identified that age, pathological stage, and risk score had a significant correlation with the patients' prognosis (P<0.001) (*Figure 3B,3C*). The distribution of risk scores and survival conditions for the high-risk and low-risk groups were presented as follows (*Figure 3D,3E*). Additionally, we assessed the predictive performance of our model using ROC curves. The AUC values for the TCGA cohort at 1 year, 3 years, and 5 years were 0.702, 0.725, and 0.668, respectively (*Figure 3F*), confirming the accuracy of our model. The results in the external validation were consistent as showing a positive correlation between mortality rate and risk score (*Figure 3G-3L*).

Association of PANoptosis risk score and clinical features

Through our association study, it was found that the risk score had no evident link with age (*Figure 4A*). However, there was a significant correlation between the risk score and tumor staging (*Figure 4B*). The relationship between the risk score, stage, and age groups is further illustrated in *Figure 4C*. Clinical feature subgroup analysis revealed that in patients aged over 60, those in the high-risk group exhibited notably poorer survival outcomes (*Figure 4D,4E*). For both early and advanced stages of the disease, the survival rate of the high-risk group was notably lower than the low-risk group (*Figure 4F,4G*).

Immune cell infiltration and tumor microenvironment analysis

Utilizing methods such as CIBERSORTx, ImmuneCellAI, and ssGSEA, we analyzed the immune cell infiltration in pMMR patients (n=330). We observed a significant difference in the Macrophages M0 immune infiltration scores between the high and low-risk groups (*Figure 5A-5C*). We also evaluated the tumor microenvironment using the TMEscore. There was a negative correlation between the TMEscore and the risk score. Patients in the high-risk group exhibited a lower TMEscore, indicating a poorer prognosis (*Figure 6A-6C*). The results from ESTIMATE indicated that StromalScore, ImmuneScore, and EstimateScore were all positively correlated with the risk score (*Figure 6D-6F*). Additionally, based on the ssGSEA analysis, the scores for angiogenesis, EMT (epithelial-mesenchymal transition), and the state of hypoxia all demonstrated a positive relationship with the risk score, indicating that patients in the high-risk group face a more unfavorable prognosis. (*Figure 6G-6I*). Lastly, when comparing the signaling pathways of the high-risk and low-risk groups, we observed distinct differences in the extracellular matrix (ECM) receptor interaction, MAPK signaling pathway, PI3K-Akt signaling pathway, and Wnt signaling pathway (*Figure 6J*).

Biological pathway enrichment analysis of PANoptosis risk score

We performed GSEA analysis on the DEGs of the high and low-risk groups. The results of the Gene Ontology (GO) enrichment analysis showed that the main increased functions were collagen fibril organization, elastic fiber assembly and collagen binding (*Figure 7A*). The main decreased functions were epithelial DNA replication initiation, structure maintenance and maintenance of gastrointestinal epithelium (*Figure 7B*). Meanwhile, the results from the KEGG functional enrichment analysis pointed out that ECM receptor interaction, glycosaminoglycan biosynthesis chondroitin sulfate and focal adhesion were the foremost enhanced biological processes (*Figure 7C*), and the main diminished functions were terpenoid backbone biosynthesis, butanoate metabolism and DNA replication (*Figure 7D*).

Association study of prognosis genes and drug reactivity

Leveraging the Cancer Therapeutics Response Portal (CTRP) database and Genomics of Drug Sensitivity in Cancer (GDSC) database, we conducted the drug sensitivity analysis. The expression levels of TIMP1, CDKN2A, and CAMK2B were found to be positively correlated with sensitivity to fluorouracil, oxaliplatin, and lapatinib. Conversely, TLR3 expression was inversely associated with sensitivity to these drugs. Consistent with these observations, the risk score analysis revealed that high-risk group demonstrated increased sensitivity to fluorouracil, oxaliplatin, and lapatinib (*Figure 8A-8C*).

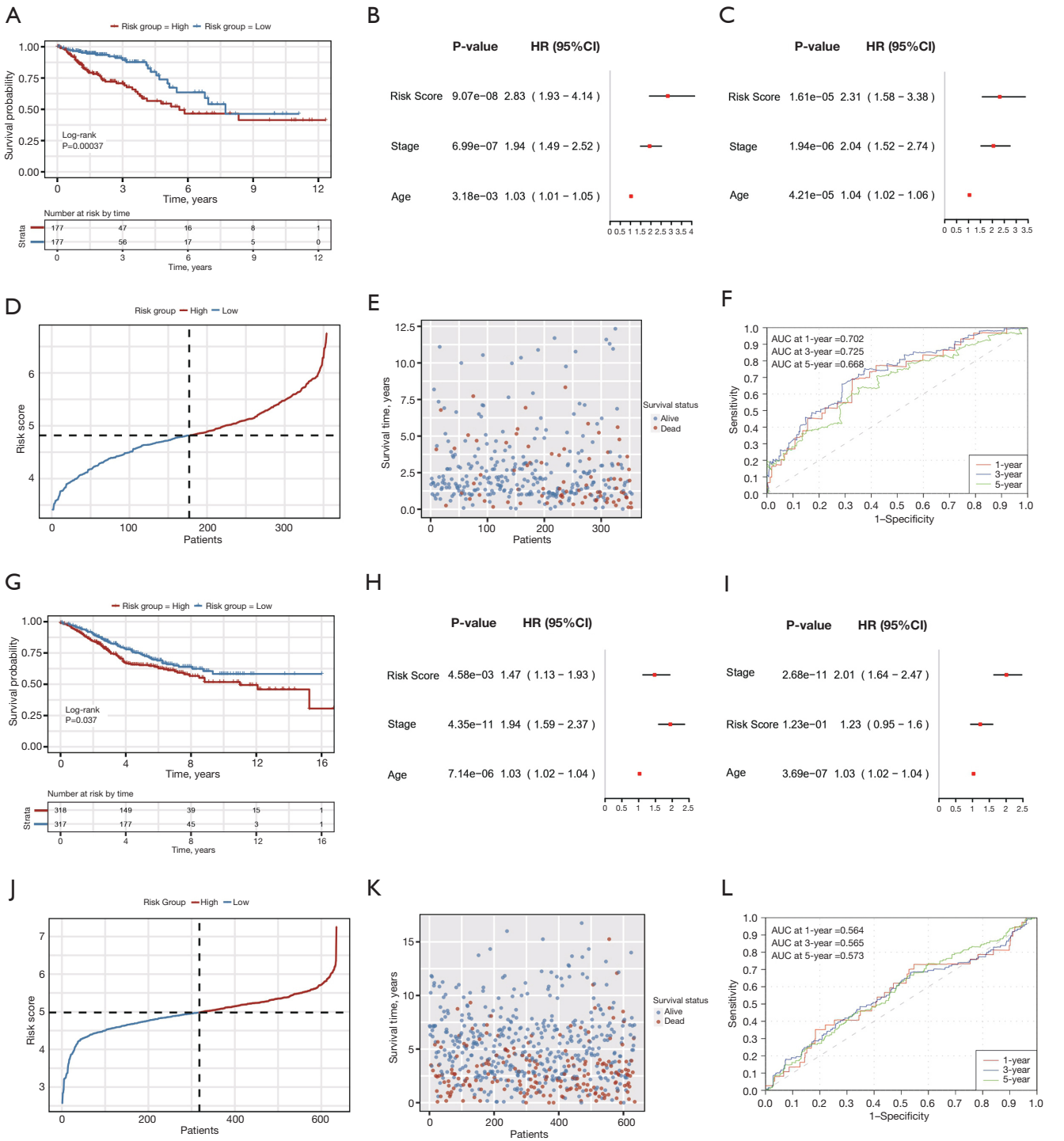

Figure 3 Construction of the prognostic risk model. (A) Kaplan-Meier survival curves of OS between low-risk and high-risk groups. (B-C) The univariate and multivariate Cox regression analysis of risk model score and clinical features regarding prognostic value. (D) Risk score distribution between high and low-risk. (E) Survival status of patients in different risk groups. (F) Time-dependent ROC curves of 1-, 3-, and 5-year of CRC patients. (G-L) Test set. HR, hazard ratio; CI, confidence interval; AUC, area under the curve; OS, overall survival; ROC, receiver operating characteristic; CRC, colorectal cancer.

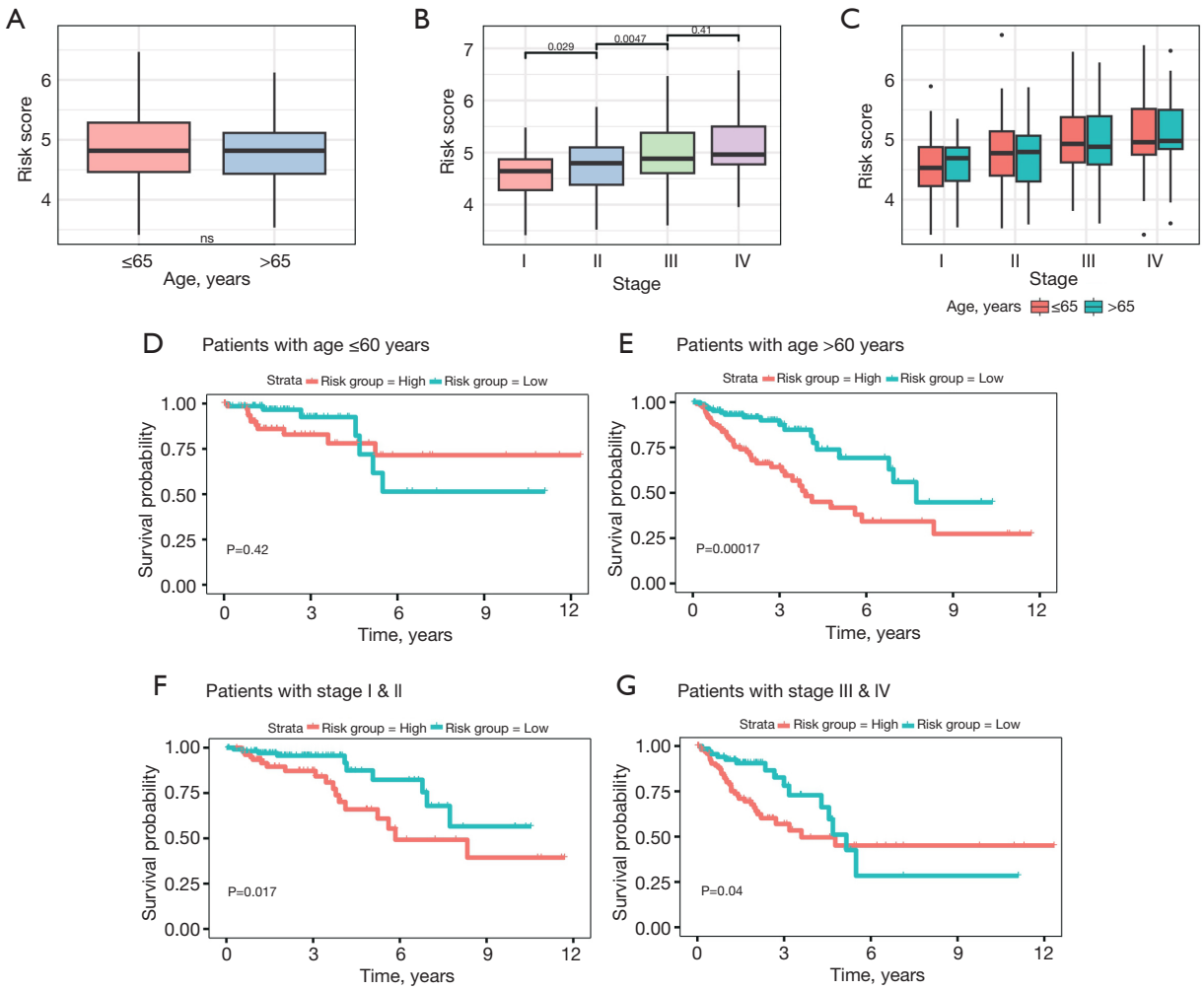

Figure 4 The relationship between risk score and other clinical variables. (A-C) Box plots of correlation between risk score and age, stage, respectively. (D-E) Survival status of patients in high and low risk groups in different age groups. (F-G) Survival status of patients in high and low risk groups in different stage groups. ns, no significance.

Discussion

Previous researches have suggested that pyroptosis, apoptosis, and necroptosis have a pivotal impact on the immune response against cancer (21-23). For instance, in breast cancer, cell pyroptosis can enhance anti-tumor immunity (24); cell apoptosis inhibits the proliferation of cancer cells; initiating the necroptosis signaling route has positive implications for tumor suppression (25). However, as research progressed, we have come to understand that there can be synergistic effects between them, further enhancing their roles. Consequently, in recent years, some research has delved into the potential role of PANoptosis in cancer therapies and its modulation methods in infectious diseases (26). Some research findings on pyroptosis and necroptosis might offer new perspectives for the future direction of cancer treatment, giving an initial explanation of the value of PANoptosis in the treatment of diverse tumors (27). For example, Pan and colleagues found that PANoptosis has a good predictive capability for the immune treatment response in gastric cancer (7). Furthermore, features related to PANoptosis have been recognized in cancers such as prostate cancer, liver cancer, breast cancer, and glioma (28-31). Nevertheless, relatively little knowledge is available related to the impact of PANoptosis on CRC. Therefore, exploring the role of PANoptosis in CRC not only provides insights into the programmed death research

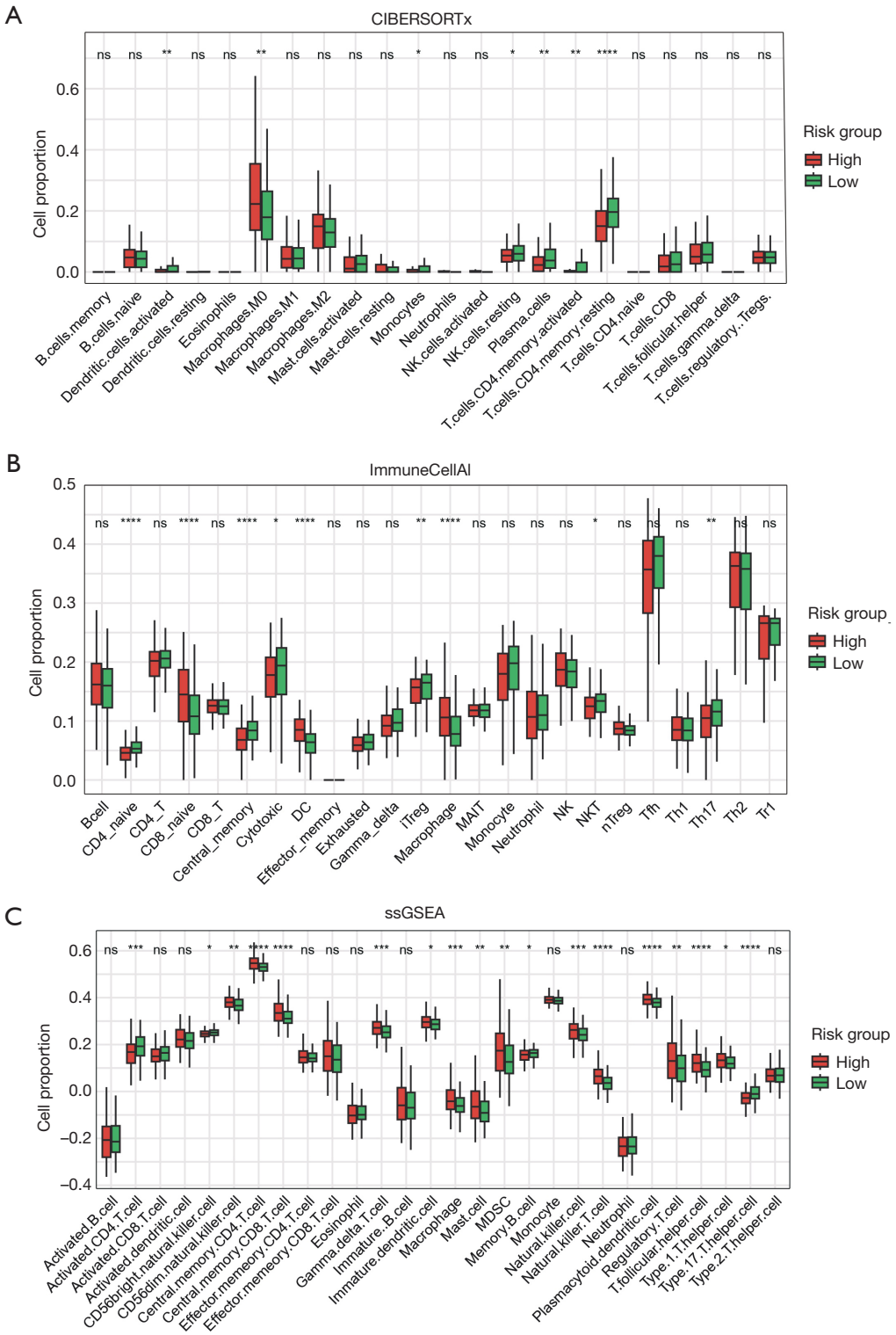

Figure 5 Immune cell infiltration. (A-C) Box plots showed the immune infiltration of immune cells calculated by CIBERSORTx, ImmuneCellAI and ssGSEA. *, P<0.05; **, P<0.01; ***, P<0.001; ****, P<0.0001; ns, no statistical significance. ssGSEA, single-sample gene set enrichment analysis.

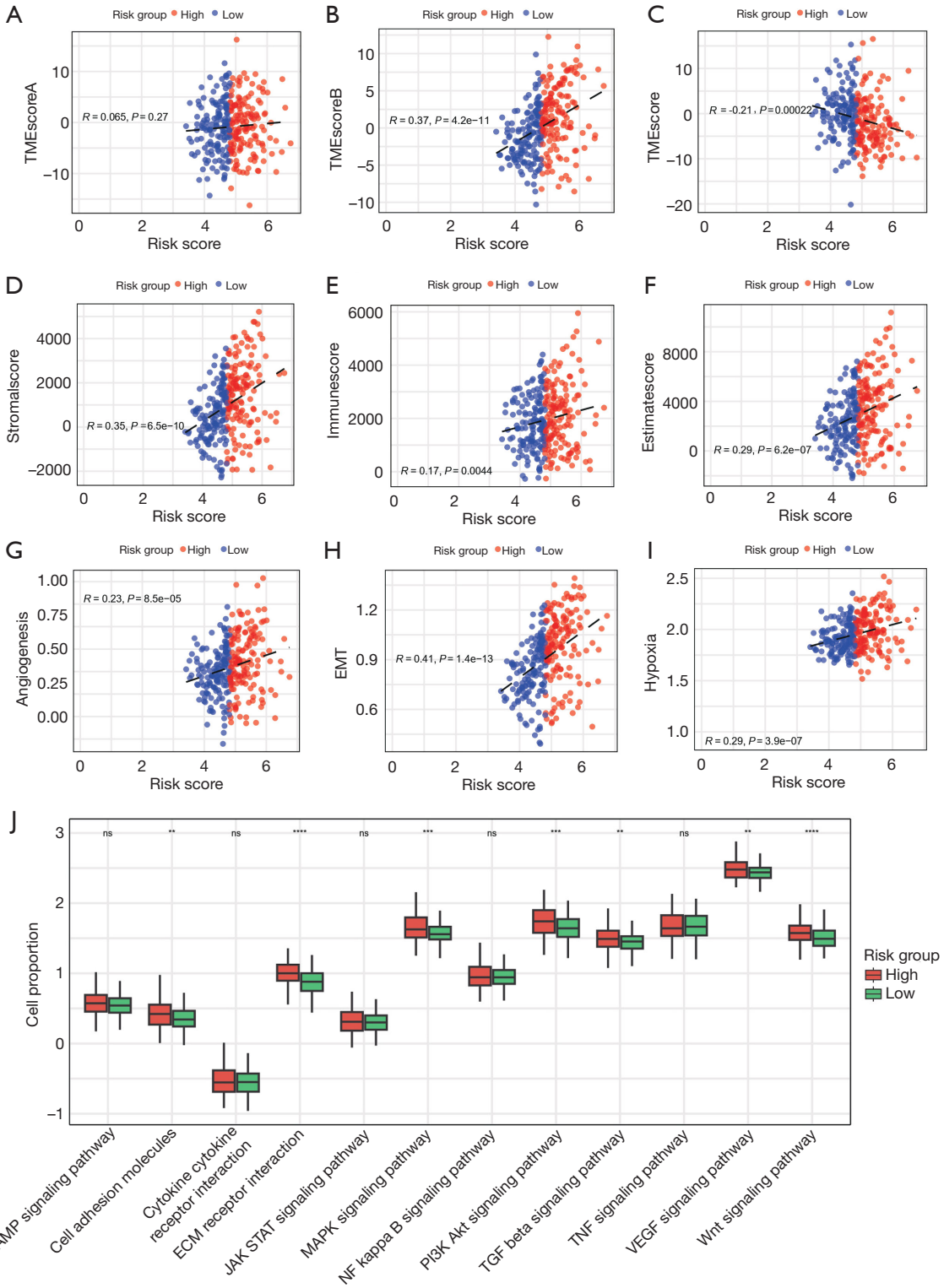

Figure 6 Tumor immune microenvironment. (A-C) Correlation analysis of risk with TMEscore. (D-F) Estimate score, immune score, and stromal score in high-risk and low-risk groups. (G-I) The risk score's correlation with angiogenic activity score, hypoxia score, and mesenchymal-EMT score. (J) The risk score's correlation with signal pathway score. **, P<0.01; ***, P<0.001; ****, P<0.0001; ns, no statistical significance. TMEscore, Tumor Microenvironment Score; EMT, epithelial-mesenchymal transition.

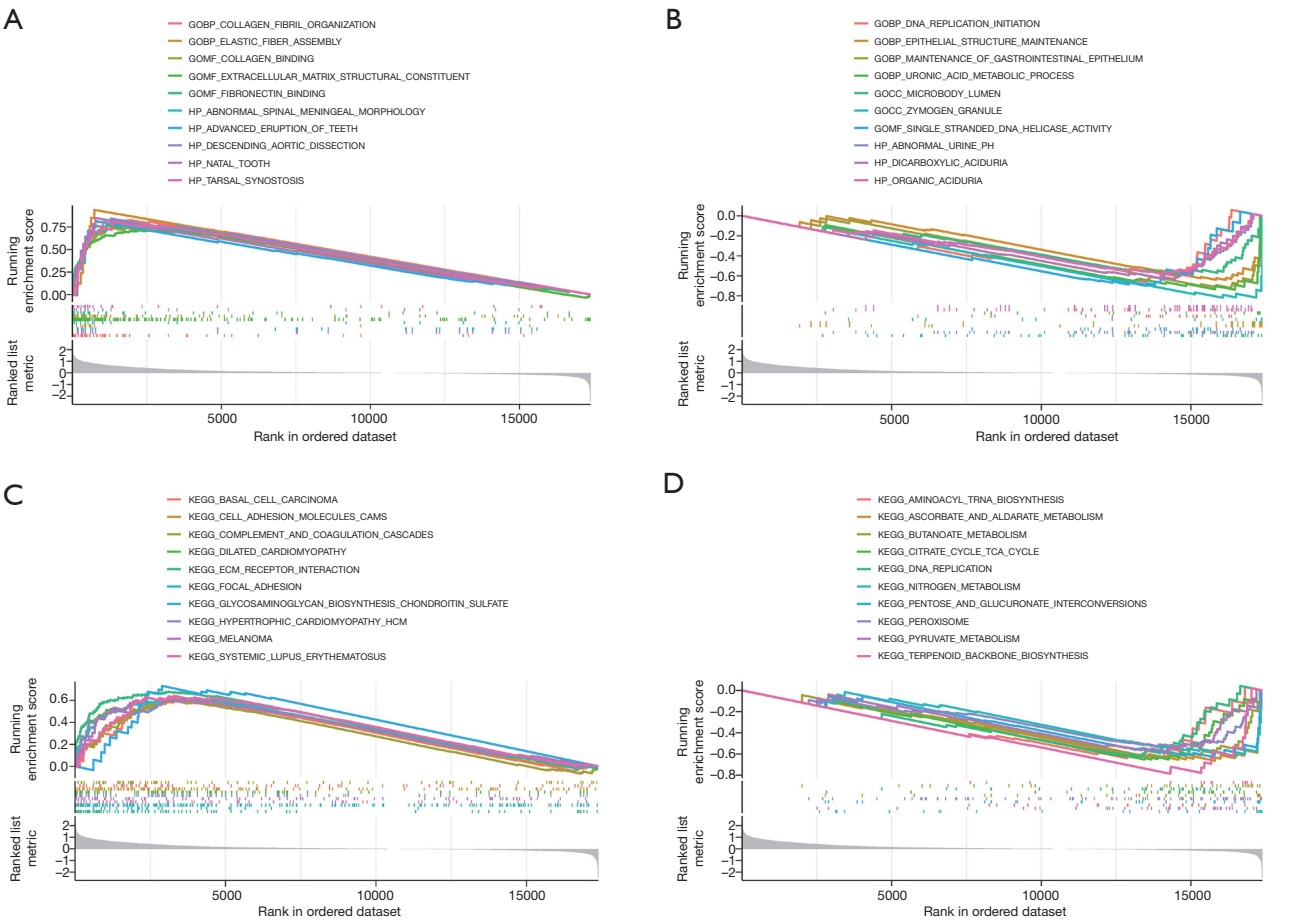

Figure 7 Enrichment analysis of DEGs. (A,B) GO enrichment analysis. (C,D) KEGG enrichment analysis. GOBP, Gene Ontology Biological Process; GOMF, Gene Ontology Molecular Function; GOCC, Gene Ontology Cellular Component; HP, Human Phenotype; KEGG, Kyoto Encyclopedia of Genes and Genomes; DEGs, differentially expressed genes.

of CRC cells, but also helps offer new directions for the therapy of patients with CRC.

In this study, the relationship between CRC and PANoptosis was explored in depth. By comprehensively analyzing the dataset of CRC patients from the TCGA database, we successfully identified DEGs related to PANoptosis and further constructed a risk scoring model predicting CRC prognosis. Our findings suggest that the DEGs related to PANoptosis hold significant biological implications in CRC. These genes are not only associated with the onset and progression of CRC but also closely linked to patient outcomes. We identified that the genes *TIMP1*, *CDKN2A*, *CAMK2B*, and *TLR3* are prognostically significant for CRC patients. Among them, inhibiting TIMP1 expression increases apoptosis of CRC cells and reduces cancer proliferation and metastasis by inducing TIMP1-specific regulation of the FAK-PI3K/AKT and MAPK pathways (32). High expression of CDKN2A in CRC leads to poor prognosis, while knocking down CDKN2A expression can promote apoptosis and cell cycle progression, affect the EMT process in CRC, and thereby inhibit cancer cell proliferation (33). Utilizing these four genes, we established a risk scoring model, providing an effective predictive tool for the prognosis of CRC patients. The predictive capability of this model was further validated through its association with other clinical features, such as age and tumor staging. We employed methods like CIBERSORTx, ImmuneCellAI, and ssGSEA to analyze the immune cell infiltration in both high- and low-risk groups. We observed a marked increase in M0 macrophage infiltration among patients in the high-risk group. This enhanced M0 macrophage immune infiltration might

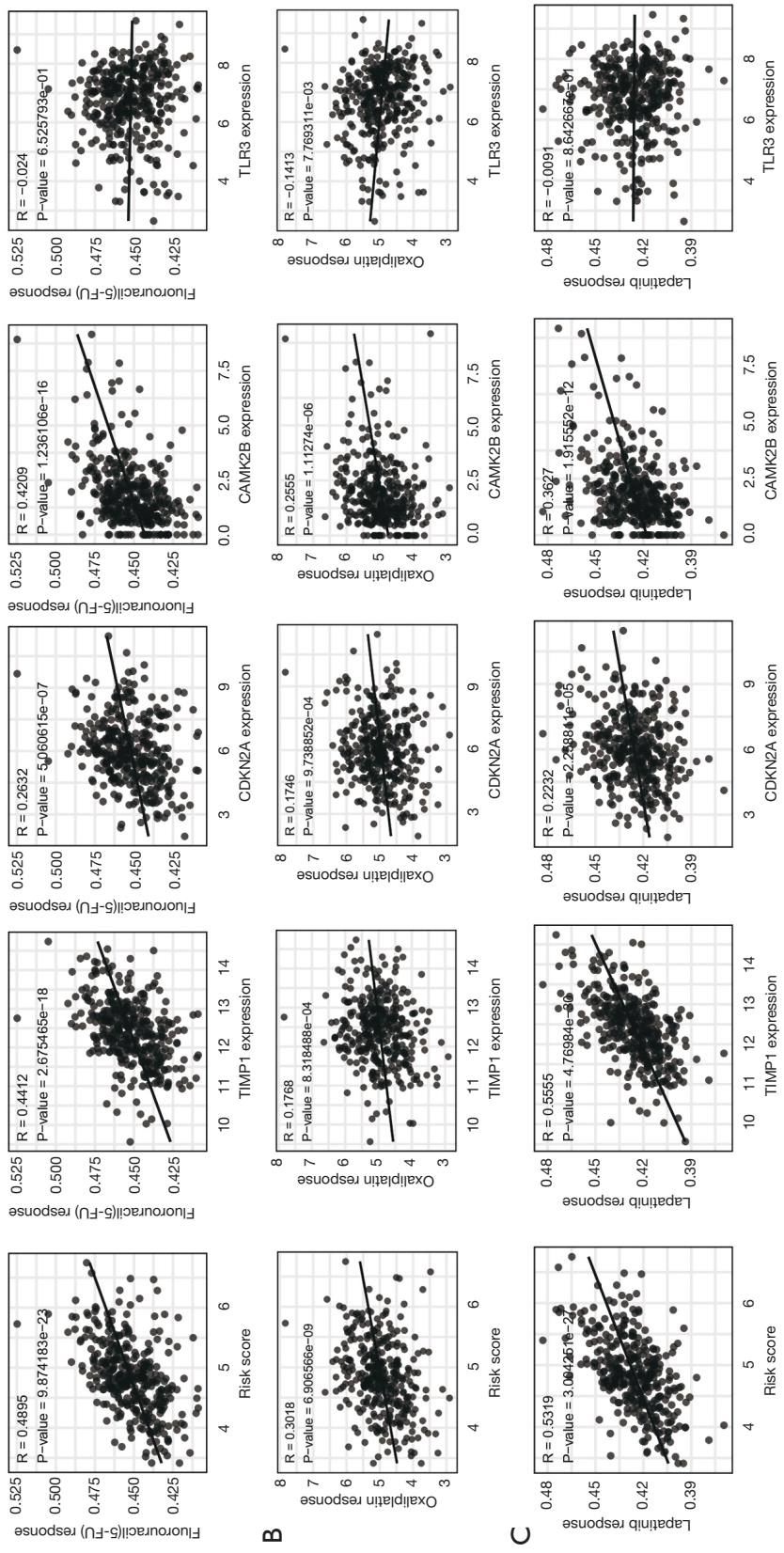

Figure 8 Drug sensitivity analysis. (A-C) Correlation analysis of risk score and feature gene expression with sensitivity to fluorouracil, oxaliplatin and lapatinib.

improve the efficacy of checkpoint inhibitor treatments, amplifying the capability of immune cells to target the tumor (34). When assessing the tumor microenvironment, the low TMEscore in the high-risk group indicates reduced immunosuppression in the tumor microenvironment, which is beneficial for immunotherapy. The elevated stromal and immune scores may signify an abundance of immune cells and stromal components, correlating positively with the effectiveness of immunotherapy. However, increased angiogenesis, epithelial-mesenchymal transition, and hypoxia levels are associated with the tumor's invasiveness, metastatic tendencies, and malignancy, potentially diminishing the efficacy of immunotherapy and allowing tumor cells to evade the immune system (35). We carried out a GSEA analysis on the differential gene expression between the high-risk and low-risk groups. The GO enrichment analysis results showed that the primary enhanced functions are collagen fibril organization, elastic fiber assembly, and collagen binding, whereas the main diminished functions are epithelial DNA replication initiation, structure maintenance, and maintenance of the gastrointestinal epithelium. Concurrently, the KEGG enrichment analysis indicated that ECM receptor interaction, glycosaminoglycan biosynthesis chondroitin sulfate, and focal adhesion are the predominant augmented biological functions, while the primary reduced functions are terpenoid backbone biosynthesis, butanoate metabolism, and DNA replication, indicating a poor prognosis (36,37). Utilizing the CTRP database and GDSC dataset, we predicted the drug sensitivity. TIMP1, CDKN2A, and CAMK2B levels positively correlated with sensitivity to fluorouracil, oxaliplatin, and lapatinib, while TLR3 showed an inverse relationship. Similarly, high-risk group exhibited greater sensitivity to these therapeutic agents.

There are certain limitations in this study. Firstly, our research primarily relies on data from the TCGA database, which might introduce some biases. In the future, we need to validate our findings in a larger patient cohort. Additionally, while our risk scoring model performed well in the training set, its performance in other independent datasets still requires further validation.

Conclusions

In summary, our analysis presents an early snapshot of the relationship between PANoptosis and CRC prognosis, and molecular signature as well. The DEGs related to PANoptosis and the risk score model we identified offer valuable tools for the diagnosis and treatment of CRC. Moving forward, we hope to further validate our findings and explore the specific roles of these genes in the pathogenesis of CRC. Our results would consequently reveal candidate targets for the diagnosis and prognosis of CRC, along with novel insights for therapeutic interventions.

Acknowledgments

Funding: This study was supported by the National Natural Science Foundation of China (No. 81472782), and the Research Fund of Yili Institute of Clinical Medicine (No. yl2021ms02).

Footnote

Reporting Checklist: The authors have completed the TRIPOD reporting checklist. Available at https://jgo.amegroups.com/article/view/10.21037/jgo-24-245/rc

Data Sharing Statement: Available at https://jgo.amegroups.com/article/view/10.21037/jgo-24-245/dss

Peer Review File: Available at https://jgo.amegroups.com/article/view/10.21037/jgo-24-245/prf

Conflicts of Interest: All authors have completed the ICMJE uniform disclosure form (available at https://jgo.amegroups.com/article/view/10.21037/jgo-24-245/coif). The authors have no conflicts of interest to declare.

Ethical Statement: The authors are accountable for all aspects of the work in ensuring that questions related to the accuracy or integrity of any part of the work are appropriately investigated and resolved. The study was conducted in accordance with the Declaration of Helsinki (as revised in 2013).

References

1. Bray F, Laversanne M, Sung H, et al. Global cancer statistics 2022: GLOBOCAN estimates of incidence and mortality worldwide for 36 cancers in 185 countries. CA Cancer J Clin 2024;74:229-63.
2. Benson AB, Venook AP, Al-Hawary MM, et al. Colon Cancer, Version 2.2021, NCCN Clinical Practice Guidelines in Oncology. J Natl Compr Canc Netw 2021;19:329-59.
3. Yaeger R, Chatila WK, Lipsyc MD, et al. Clinical Sequencing Defines the Genomic Landscape of Metastatic Colorectal Cancer. Cancer Cell 2018;33:125-136.e3.
4. Li C, Sun YD, Yu GY, et al. Integrated Omics of Metastatic Colorectal Cancer. Cancer Cell 2020;38:734-747.e9.
5. van der Stok EP, Spaander MCW, Grünhagen DJ, et al. Surveillance after curative treatment for colorectal cancer. Nat Rev Clin Oncol 2017;14:297-315.
6. Malireddi RKS, Kesavardhana S, Kanneganti TD. ZBP1 and TAK1: Master Regulators of NLRP3 Inflammasome/Pyroptosis, Apoptosis, and Necroptosis (PAN-optosis). Front Cell Infect Microbiol 2019;9:406.
7. Pan H, Pan J, Li P, et al. Characterization of PANoptosis patterns predicts survival and immunotherapy response in gastric cancer. Clin Immunol 2022;238:109019.
8. Chen W, Gullett JM, Tweedell RE, et al. Innate immune inflammatory cell death: PANoptosis and PANoptosomes in host defense and disease. Eur J Immunol 2023;53:e2250235.
9. Lee E, Song CH, Bae SJ, et al. Regulated cell death pathways and their roles in homeostasis, infection, inflammation, and tumorigenesis. Exp Mol Med 2023;55:1632-43.
10. Zheng M, Karki R, Vogel P, et al. Caspase-6 Is a Key Regulator of Innate Immunity, Inflammasome Activation, and Host Defense. Cell 2020;181:674-687.e13.
11. Ren L, Yang Y, Li W, et al. CDK1 serves as a therapeutic target of adrenocortical carcinoma via regulating epithelial-mesenchymal transition, G2/M phase transition, and PANoptosis. J Transl Med 2022;20:444.
12. Liu X, Xie X, Ren Y, et al. The role of necroptosis in disease and treatment. MedComm (2020) 2021;2:730-55.
13. Seifert L, Werba G, Tiwari S, et al. The necrosome promotes pancreatic oncogenesis via CXCL1 and Mincle-induced immune suppression. Nature 2016;532:245-9.
14. Hanahan D, Weinberg RA. Hallmarks of cancer: the next generation. Cell 2011;144:646-74.
15. Karki R, Sundaram B, Sharma BR, et al. ADAR1 restricts ZBP1-mediated immune response and PANoptosis to promote tumorigenesis. Cell Rep 2021;37:109858.
16. Muendlein HI, Connolly WM, Magri Z, et al. ZBP1 promotes inflammatory responses downstream of TLR3/TLR4 via timely delivery of RIPK1 to TRIF. Proc Natl Acad Sci U S A 2022;119:e2113872119.
17. Malireddi RKS, Karki R, Sundaram B, et al. Inflammatory Cell Death, PANoptosis, Mediated by Cytokines in Diverse Cancer Lineages Inhibits Tumor Growth. Immunohorizons 2021;5:568-80.
18. Zhu P, Ke ZR, Chen JX, et al. Advances in mechanism and regulation of PANoptosis: Prospects in disease treatment. Front Immunol 2023;14:1120034.
19. Liu LX, Heng JH, Deng DX, et al. Sulconazole Induces PANoptosis by Triggering Oxidative Stress and Inhibiting Glycolysis to Increase Radiosensitivity in Esophageal Cancer. Mol Cell Proteomics 2023;22:100551.
20. Du M, Gu D, Xin J, et al. Integrated multi-omics approach to distinct molecular characterization and classification of early-onset colorectal cancer. Cell Rep Med 2023;4:100974.
21. Ke J, Zhao F, Luo Y, et al. MiR-124 Negatively Regulated PARP1 to Alleviate Renal Ischemia-reperfusion Injury by Inhibiting TNFα/RIP1/RIP3 Pathway. Int J Biol Sci 2021;17:2099-111.
22. Yan H, Luo B, Wu X, et al. Cisplatin Induces Pyroptosis via Activation of MEG3/NLRP3/caspase-1/GSDMD Pathway in Triple-Negative Breast Cancer. Int J Biol Sci 2021;17:2606-21.
23. Liu Z, Li Y, Zhu Y, et al. Apoptin induces pyroptosis of colorectal cancer cells via the GSDME-dependent pathway. Int J Biol Sci 2022;18:717-30.
24. Wang H, Rong X, Zhao G, et al. The microbial metabolite trimethylamine N-oxide promotes antitumor immunity in triple-negative breast cancer. Cell Metab 2022;34:581-594.e8.
25. Khorsandi L, Orazizadeh M, Niazvand F, et al. Quercetin induces apoptosis and necroptosis in MCF-7 breast cancer cells. Bratisl Lek Listy 2017;118:123-8.
26. Banoth B, Tuladhar S, Karki R, et al. ZBP1 promotes fungi-induced inflammasome activation and pyroptosis, apoptosis, and necroptosis (PANoptosis). J Biol Chem 2020;295:18276-83.
27. Lin JF, Hu PS, Wang YY, et al. Phosphorylated NFS1 weakens oxaliplatin-based chemosensitivity of colorectal cancer by preventing PANoptosis. Signal Transduct Target Ther 2022;7:54.

28. Zhu J, Huang Q, Peng X, et al. Identification of molecular subtypes based on PANoptosis-related genes and construction of a signature for predicting the prognosis and response to immunotherapy response in hepatocellular carcinoma. Front Immunol 2023;14:1218661.
29. Yi X, Li J, Zheng X, et al. Construction of PANoptosis signature: Novel target discovery for prostate cancer immunotherapy. Mol Ther Nucleic Acids 2023;33:376-90.
30. Song J, Xu Z, Fan Q, et al. The PANoptosis-related signature indicates the prognosis and tumor immune infiltration features of gliomas. Front Mol Neurosci 2023;16:1198713.
31. He P, Ma Y, Wu Y, et al. Exploring PANoptosis in breast cancer based on scRNA-seq and bulk-seq. Front Endocrinol (Lausanne) 2023;14:1164930.
32. Song G, Xu S, Zhang H, et al. TIMP1 is a prognostic marker for the progression and metastasis of colon cancer through FAK-PI3K/AKT and MAPK pathway. J Exp Clin Cancer Res 2016;35:148.
33. Shi WK, Li YH, Bai XS, et al. The Cell Cycle-Associated Protein CDKN2A May Promotes Colorectal Cancer Cell Metastasis by Inducing Epithelial-Mesenchymal Transition. Front Oncol 2022;12:834235.
34. Shibutani M, Nakao S, Maeda K, et al. The Impact of Tumor-associated Macrophages on Chemoresistance via Angiogenesis in Colorectal Cancer. Anticancer Res 2021;41:4447-53.
35. Zeng D, Li M, Zhou R, et al. Tumor Microenvironment Characterization in Gastric Cancer Identifies Prognostic and Immunotherapeutically Relevant Gene Signatures. Cancer Immunol Res 2019;7:737-50.
36. Durinikova E, Reilly NM, Buzo K, et al. Targeting the DNA Damage Response Pathways and Replication Stress in Colorectal Cancer. Clin Cancer Res 2022;28:3874-89.
37. IJsselsteijn ME, Sanz-Pamplona R, Hermitte F, et al. Colorectal cancer: A paradigmatic model for cancer immunology and immunotherapy. Mol Aspects Med 2019;69:123-9.

Cite this article as: Zhao T, Zhang X, Liu X, Jiang X, Chen S, Li H, Ji H, Wang S, Liang Q, Ni S, Du M, Liu L. Characterizing PANoptosis gene signature in prognosis and chemosensitivity of colorectal cancer. J Gastrointest Oncol 2024;15(5):2129-2144. doi: 10.21037/jgo-24-245

Supplementary

Table S1 Clinical pathological parameters of CRC

Clinical	Characteristics	TCGA		GSE39582		NJCRC	
		N	Percent	N	Percent	N	Percent
Age (years)	Average	64.9		66.9		58.7	
Gender	Female	187	46.29%	260	44.91%	25	44.64%
	Male	217	53.71%	319	55.09%	31	55.36%
Stage	I	64	15.84%	38	6.56%	2	3.57%
	II	158	39.11%	269	46.46%	29	51.79%
	III	121	29.95%	209	36.10%	24	42.86%
	IV	61	15.10%	61	10.54%	1	1.78%
MMR	pMMR	330	81.68%	460	79.45%		
	dMMR	59	14.60%	73	12.61%		
	unknown	15	3.71%	46	7.94%		

CRC, colorectal cancer; TCGA, The Cancer Genome Atlas; NJCRC, Nanjing Colorectal Cancer; MMR, mismatch repair.

https://dx.doi.org/10.21037/jgo-24-245

Table S2 PANoptosis-related genes

KEGG_NECROPTOSIS	REACTOME_PYROPTOSIS	KEGG_APOPTOSIS	HALLMARK_APOPTOSIS	REACTOME_APOPTOSIS
TNF	*BAK1*	*CASP10*	*CASP3*	*BAD*
TNFRSF1A	*TNK3*	*CASP9*	*CASP9*	*CFLAR*
TRADD	*CHMP2B*	*CASP8*	*DFFA*	*PSMB1*
TRAF2	*BAX*	*CASP7*	*CASP7*	*PSMC4*
TRAF5	*GZMB*	*CHUK*	*CFLAR*	*BID*
RIPK1	*CHMP4B*	*PRKAR2B*	*BIRC3*	*VIM*
BIRC2	*GSDMD*	*TNF*	*PMAIP1*	*FAS*
BIRC3	*GSDME*	*TNFSF10*	*CASP8*	*BAK1*
XIAP	*IL1A*	*BIRC3*	*JUN*	*DAPK2*
RBCK1	*CHMP3*	*XIAP*	*BCL2L11*	*CDH1*
RNF31	*IRF1*	*PPP3R2*	*MCL1*	*PSMA4*
SHARPIN	*IL1B*	*PPP3CC*	*IL1B*	*DSG2*
SPATA2L	*CHMP2A*	*PPP3R1*	*SPTAN1*	*CASP8*
SPATA2	*CASP1*	*MYD88*	*DIABLO*	*PRKCQ*
CYLD	*CASP5*	*FADD*	*BAX*	*ROCK1*
FADD	*TP53*	*CFLAR*	*BIK*	*PSME4*
CASP8	*CHMP7*	*RIPK1*	*IL1A*	*ARHGAP10*
CFLAR	*IL18*	*BAD*	*BID*	*TP63*
RIPK3	*CASP3*	*IRAK4*	*CDKN1A*	*TP73*
CYBB	*CHMP4C*	*BID*	*GADD45A*	*PKP1*
CAMK2A	*IRF2*	*BAX*	*DDIT3*	*BAX*
CAMK2D	*CYCS*	*IKBKB*	*CDKN1B*	*PSMC5*
CAMK2B	*CHMP6*	*CASP6*	*TNF*	*AOD1*
CAMK2G	*HMGB1*	*IL1A*	*GSN*	*DNM1L*
SLC25A4	*CASP4*	*AKT1*	*TNFSF10*	*PPP1R13B*
SLC25A5	*ELANE*	*CASP3*	*CASP6*	*DYNLL1*
SLC25A6	*CHMP4A*	*AKT2*	*SQSTM1*	*PSME1*
SLC25A31		*TNFRSF1A*	*FASLG*	*CLSPN*
PPID		*AKT3*	*EGR3*	*PSMD5*
VDAC1		*CHP2*	*CD44*	*DSP*
VDAC2		*ATM*	*FAS*	*PSMD8*
VDAC3		*ENDOG*	*IL18*	*MAPK1*
GLUD2		*NFKB1*	*IGFBP6*	*GZMB*
GLUD1		*NFKBIA*	*PRF1*	*PSMC6*
GLUL		*CAPN2*	*DAP*	*PSMA3*
PYGL		*PIK3R5*	*CCND1*	*PSMC1*
PYGM		*IKBKG*	*BTG3*	*PSMB5*
PYGB		*CAPN1*	*F2R*	*ACIN1*
MAPK8		*IL3RA*	*SATB1*	*PSMA6*
MAPK10		*IL3*	*BNIP3L*	*PSME2*
MAPK9		*RELA*	*CASP4*	*PSMA7*
FTH1		*ENDOD1*	*TNFRSF12A*	*E2F1*
FTL		*APAF1*	*CREBBP*	*PSMD10*
PLA2G4E		*PRKX*	*RHOB*	*XIAP*
PLA2G4A		*CSF2RB*	*GPX3*	*BMX*
JMJD7-PLA2G4B		*TNFRSF10A*	*PDGFRB*	*STK24*
PLA2G4B		*TRAF2*	*TSPO*	*TRADD*
PLA2G4C		*TNFRSF10D*	*CCND2*	*MAPK3*
PLA2G4D		*NGF*	*XIAP*	*PSMD7*
PLA2G4F		*TNFRSF10B*	*TIMP1*	*TJP1*
ALOX15		*TNFRSF10C*	*CTNNB1*	*BMF*
CAPN1		*MAP3K14*	*IRF1*	*GSDMD*
CAPN2		*IL1RAP*	*HSPB1*	*TNFRSF10A*
SMPD1		*IL1B*	*AOD1*	*AKT2*
MLKL		*IRAK2*	*TIMP2*	*BBC3*
PGAM5		*IL1R1*	*BTG2*	*CARD8*
DNM1L		*IRAK1*	*TIMP3*	*GSDME*
NLRP3		*TRADD*	*LEF1*	*PSMA2*
PYCARD		*PIK3R3*	*CASP1*	*MAPK8*
CASP1		*BCL2*	*GPX1*	*UNC5B*
IL1B		*BCL2L1*	*BCL10*	*PSMD3*
CHMP2A		*BIRC2*	*IGF2R*	*SEPTIN4*
CHMP2B		*IRAK3*	*CDC25B*	*KPNB1*
CHMP3		*PRKACA*	*AIFM3*	*C1QBP*
RNF103-CHMP3		*PRKACB*	*CD38*	*PSMD11*
CHMP4B		*PRKACG*	*PPP3R1*	*YWHAE*
CHMP4A		*PPP3CB*	*HGF*	*BIRC2*
CHMP6		*TP53*	*CLU*	*PSMD9*
VPS4B		*PPP3CA*	*ATF3*	*LMNB1*
VPS4A		*PIK3CA*	*LGALS3*	*UNC5A*
CHMP1B		*PIK3CB*	*LUM*	*KPNA1*
CHMP1A		*FAS*	*LMNA*	*TFDP2*
CHMP5		*DFFA*	*GADD45B*	*PSMD14*
CHMP7		*CYCS*	*CDK2*	*AKT3*
TRPM7		*DFFB*	*IFNB1*	*FASLG*
IL1A		*PIK3CD*	*RETSAT*	*TJP2*
IL33		*PRKAR1A*	*SMAD7*	*APAF1*
HMGB1		*FASLG*	*SOD1*	*TNFRSF10B*
TNFSF10		*PRKAR2A*	*PTK2*	*PPP3CC*
TNFRSF10A		*PRKAR1B*	*ENO2*	*TNFSF10*
TNFRSF10B		*EXOG*	*HMOX1*	*H1-3*
FASLG		*PIK3CG*	*IER3*	*H1-1*
FAS		*AIFM1*	*BCL2L10*	*PSMF1*
FAF1		*NTRK1*	*CD2*	*PSMB2*
IFNA1		*PIK3R1*	*GCH1*	*TRAF2*
IFNA2		*PIK3R2*	*MMP2*	*TICAM1*
IFNA4		*CHP1*	*VDAC2*	*SEM1*
IFNA5			*TAP1*	*YWHAH*
IFNA6			*PLAT*	*PSMA1*
IFNA7			*IFNGR1*	*PSME3*
IFNA8			*APP*	*CASP9*
IFNA10			*BRCA1*	*YWHAQ*
IFNA13			*ROCK1*	*STK26*
IFNA14			*PSEN1*	*DSG3*
IFNA16			*DCN*	*DSG1*
IFNA17			*PSEN2*	*APC*
IFNA21			*SOD2*	*DBNL*
IFNB1			*BMF*	*NMT1*
IFNG			*EREG*	*TLR4*
IFNAR1			*KRT18*	*PSMB7*
IFNAR2			*TGFB2*	*RIPK1*
IFNGR1			*RELA*	*UACA*
IFNGR2			*WEE1*	*CASP6*
JAK1			*RARA*	*TP53*
JAK2			*CD14*	*PMAIP1*
JAK3			*CD69*	*AKT1*
TYK2			*PEA15*	*PSMB6*
STAT1			*DNAJC3*	*PSMA5*
STAT2			*CASP2*	*TP53BP2*
STAT3			*CTH*	*RPS27A*
STAT4			*PLCB2*	*CDKN2A*
STAT5A			*BMP2*	*GSN*
STAT5B			*HMGB2*	*GAS2*
STAT6			*PLPPR4*	*APIP*
IRF9			*H1-0*	*UBC*
EIF2AK2			*TGFBR3*	*BCL2L11*
TLR4			*EBP*	*LY96*
TICAM2			*TXNIP*	*PSMA8*
TICAM1			*ANKH*	*APPL1*
TLR3			*RHOT2*	*PSMD4*
ZBP1			*CYLD*	*PSMB4*
USP21			*GSTM1*	*DFFA*
SQSTM1			*GSR*	*LMNA*
HSP90AA1			*BGN*	*PSMC2*
HSP90AB1			*BCL2L1*	*OMA1*
TNFAIP3			*GNA15*	*PSMD6*
PARP2			*MGMT*	*PRKCD*
PARP3			*PPT1*	*HMGB2*
PARP4			*F2*	*CASP3*
BID			*IL6*	*YWHAZ*
BAX			*SC5D*	*CASP7*
AIFM1			*IFITM3*	*PSMC3*
H2AX			*RNASEL*	*YWHAB*
H2AC20			*EMP1*	*DAPK3*
H2AC12			*CAV1*	*CTNNB1*
H2AC1			*DNM1L*	*FADD*
H2AW			*ANXA1*	*H1-4*
H2AB3			*TOP2A*	*FNTA*
H2AC8			*ISG20*	*STAT3*
H2AC4			*SLC20A1*	*PTK2*
MACROH2A2			*MADD*	*DFFB*
MACROH2A1			*PPP2R5B*	*AVEN*
H2AC19			*BCAP31*	*YWHAG*
H2AJ			*ERBB3*	*UBB*
H2AB1			*NEDD9*	*CD14*
H2AC17			*SAT1*	*BCL2L1*
H2AC18			*PDCD4*	*BCL2*
H2AC11			*BCL2L2*	*CYCS*
H2AC21			*FEZ1*	*PSMD1*
H2AZ2			*ERBB2*	*PSMD2*
H2AC7			*DNAJA1*	*SFN*
H2AZ1			*DAP3*	*PLEC*
H2AC15			*DPYD*	*MAGED1*
H2AC6			*NEFH*	*PAK2*
H2AC13			*PAK1*	*SATB1*
H2AC14			*FDXR*	*DIABLO*
H2AC16			*GPX4*	*H1-5*
H2AB2			*ETF1*	*PSMD13*
PPIA			*CCNA1*	*BCAP31*
BCL2			*GUCY2D*	*MAPT*
			AVPR1A	*DCC*
				H1-2
				H1-0
				HMGB1
				DAPK1
				PSMD12
				SPTAN1
				OCLN
				TFDP1
				OPA1
				PSMB8
				PSMB10
				PPP3R1
				UBAS2
				PSMB11
				PSMB9
				TICAM2
				DYNLL2
				PSMB3

https://dx.doi.org/10.21037/gpo-24-245

Table S3 88 PANoptosis-related differentially expressed genes.

Gene	logFC	AveExpr	t	P value	adj.P.Val	B	Type
ELANE	–2.791	0.875	–25.323	2.15E–85	9.57E–83	184.116	Down
RETSAT	–1.799	11.253	–20.818	6.53E–66	1.45E–63	139.391	Down
PDCD4	–1.833	11.206	–20.265	1.70E–63	2.51E–61	133.848	Down
TNFRSF12A	2.461	9.771	19.579	1.70E–60	1.89E–58	126.958	Up
ENDOD1	–1.659	10.134	–18.849	2.65E–57	2.35E–55	119.631	Down
HSP90AB1	1.094	14.878	18.138	3.33E–54	2.47E–52	112.517	Up
CDC25B	2.002	11.281	17.089	1.18E–49	7.49E–48	102.078	Up
CCND1	1.599	12.073	17.045	1.83E–49	1.02E–47	101.641	Up
CASP7	–1.590	10.476	–16.180	9.60E–46	4.74E–44	93.108	Down
SMPD1	–1.822	9.152	–16.166	1.10E–45	4.88E–44	92.973	Down
E2F1	1.621	9.047	15.311	4.77E–42	1.76E–40	84.631	Up
PMAIP1	1.812	7.828	14.907	2.38E–40	8.15E–39	80.735	Up
TOP2A	1.480	11.649	14.743	1.16E–39	3.62E–38	79.157	Up
TIMP1	1.849	12.161	14.737	1.22E–39	3.62E–38	79.107	Up
GSN	–2.000	12.619	–14.558	6.87E–39	1.91E–37	77.389	Down
PYGM	–3.664	3.696	–14.437	2.18E–38	5.69E–37	76.240	Down
BMX	–3.422	3.743	–14.202	2.06E–37	5.09E–36	74.003	Down
MAPK3	–1.153	11.276	–13.768	1.26E–35	2.69E–34	69.911	Down
GPX3	–2.677	8.888	–13.227	1.98E–33	3.82E–32	64.879	Down
CHP2	–5.476	7.949	–13.215	2.21E–33	4.09E–32	64.771	Down
BRCA1	1.251	8.998	12.935	2.92E–32	4.80E–31	62.204	Up
CD44	1.157	12.573	12.678	3.09E–31	4.74E–30	59.856	Up
RNASEL	–1.235	8.113	–12.621	5.20E–31	7.69E–30	59.340	Down
MAPK10	–2.446	4.265	–12.304	9.13E–30	1.23E–28	56.492	Down
TRAF5	1.408	9.908	12.293	1.01E–29	1.32E–28	56.387	Up
PRKACB	–2.214	9.906	–12.284	1.10E–29	1.39E–28	56.307	Down
TNFSF10	–1.364	10.455	–12.265	1.30E–29	1.61E–28	56.138	Down
TLR3	–2.143	6.991	–12.043	9.48E–29	1.14E–27	54.166	Down
CAPN2	–1.158	12.213	–11.908	3.15E–28	3.58E–27	52.974	Down
IGFBP6	–2.293	7.072	–11.867	4.53E–28	5.02E–27	52.612	Down
BMP2	–2.150	8.223	–11.840	5.79E–28	6.28E–27	52.367	Down
CAMK2A	–1.883	2.381	–11.658	2.88E–27	3.05E–26	50.773	Down
LEF1	2.092	7.659	11.644	3.25E–27	3.36E–26	50.653	Up
TNFRSF10B	1.175	10.646	11.363	3.78E–26	3.65E–25	48.216	Up
BCL2	–1.820	7.375	–11.266	8.71E–26	8.23E–25	47.389	Down
HMOX1	–1.644	9.065	–11.230	1.19E–25	1.10E–24	47.080	Down
IFITM3	1.341	12.986	10.861	2.80E–24	2.49E–23	43.944	Up
LGALS3	–1.217	13.923	–10.809	4.32E–24	3.76E–23	43.514	Down
CLU	–2.547	9.965	–10.760	6.55E–24	5.38E–23	43.102	Down
PRKAR2B	–2.319	6.746	–10.713	9.77E–24	7.88E–23	42.705	Down
SLC20A1	–1.018	10.318	–10.652	1.63E–23	1.29E–22	42.198	Down
EMP1	–1.735	11.063	–10.525	4.69E–23	3.59E–22	41.148	Down
TXNIP	–1.545	13.028	–10.393	1.41E–22	1.05E–21	40.058	Down
PKP1	3.056	6.523	10.392	1.42E–22	1.05E–21	40.053	Up
CAV1	–1.759	9.626	–10.355	1.92E–22	1.38E–21	39.749	Down
BGN	2.304	11.694	10.303	2.96E–22	2.09E–21	39.321	Up
CLSPN	1.415	6.997	10.046	2.41E–21	1.60E–20	37.243	Up
CDKN1A	–1.311	11.488	–9.899	7.92E–21	4.82E–20	36.064	Down
FAS	–1.431	8.162	–9.610	7.96E–20	4.44E–19	33.779	Down
DPYD	–2.159	6.818	–9.389	4.50E–19	2.30E–18	32.064	Down
PIK3CG	–2.212	5.419	–9.273	1.11E–18	5.56E–18	31.171	Down
CASP5	–2.306	6.192	–9.126	3.43E–18	1.62E–17	30.054	Down
IRAK2	1.427	7.801	8.925	1.58E–17	7.25E–17	28.542	Up
DCN	–2.082	11.538	–8.770	5.07E–17	2.25E–16	27.393	Down
MAPT	–2.324	4.414	–8.732	6.69E–17	2.94E–16	27.118	Down
FEZ1	–1.484	6.398	–8.542	2.72E–16	1.16E–15	25.731	Down
CAMK2B	–1.906	2.152	–8.472	4.54E–16	1.92E–15	25.226	Down
NEFH	–1.594	3.541	–8.394	8.05E–16	3.37E–15	24.661	Down
TP73	1.856	5.178	8.257	2.16E–15	8.78E–15	23.689	Up
CCNA1	–1.023	0.835	–8.248	2.30E–15	9.30E–15	23.623	Down
DSG1	1.580	2.663	8.194	3.38E–15	1.34E–14	23.244	Up
CD14	–1.336	9.636	–7.663	1.36E–13	4.96E–13	19.602	Down
GAS2	1.608	4.735	7.627	1.74E–13	6.22E–13	19.362	Up
NEDD9	–1.026	10.299	–7.508	3.87E–13	1.36E–12	18.574	Down
IL1A	1.984	4.170	7.421	6.95E–13	2.39E–12	17.998	Up
DSG3	3.188	5.279	7.404	7.77E–13	2.65E–12	17.889	Up
CD69	–1.614	5.580	–7.220	2.60E–12	8.76E–12	16.700	Down
CDKN2A	1.613	5.805	6.932	1.65E–11	5.38E–11	14.888	Up
TNFRSF10C	1.222	5.258	6.891	2.14E–11	6.87E–11	14.634	Up
CSF2RB	–1.512	7.555	–6.876	2.35E–11	7.50E–11	14.541	Down
IER3	1.016	11.834	6.699	7.06E–11	2.21E–10	13.462	Up
GZMB	1.768	6.751	6.629	1.09E–10	3.37E–10	13.040	Up
STAT4	–1.212	4.720	–6.553	1.73E–10	5.21E–10	12.586	Down
PIK3R5	–1.315	6.203	–6.522	2.08E–10	6.16E–10	12.403	Down
LY96	–1.274	5.043	–6.483	2.62E–10	7.66E–10	12.177	Down
PIK3CD	–1.197	7.276	–6.464	2.94E–10	8.48E–10	12.064	Down
AIFM3	–1.640	8.646	–6.427	3.68E–10	1.04E–09	11.844	Down
BCL2L10	–1.332	3.154	–6.389	4.61E–10	1.30E–09	11.624	Down
TGFBR3	–1.110	8.584	–5.939	6.20E–09	1.60E–08	9.086	Down
CD38	–1.575	4.840	–5.617	3.62E–08	8.54E–08	7.371	Down
DAPK1	–1.276	8.158	–5.467	8.02E–08	1.85E–07	6.597	Down
ARHGAP10	–1.132	6.940	–5.441	9.20E–08	2.11E–07	6.464	Down
AKT3	–1.042	7.316	–5.338	1.57E–07	3.57E–07	5.944	Down
F2	1.322	1.607	5.331	1.63E–07	3.65E–07	5.910	Up
CYBB	–1.045	8.959	–4.870	1.61E–06	3.23E–06	3.699	Down
GSTM1	–2.264	4.627	–4.670	4.10E–06	8.13E–06	2.798	Down
EREG	1.802	8.633	4.600	5.68E–06	1.09E–05	2.486	Up
PLA2G4A	–1.204	6.613	–3.765	0.000191342	0.000326753	–0.862	Down

https://dx.doi.org/10.21037/jgo-24-245